

Predicting quantum many-body dynamics with Long Short-Term Memory based neural networks

Zewang Zhang,¹ Shuo Yang,² Chenxi Liu,¹ Yimin Han,¹ Ching Hua Lee,^{3,4} Zheng Sun,¹ Guangjie Li,¹ and Xiao Zhang^{1,*}

¹*School of Physics, Sun Yat-sen University, Guangzhou 510275, China*

²*State Key Laboratory of Low-Dimensional Quantum Physics and Department of Physics, Tsinghua University, Beijing 100084, China*

³*Department of Physics, National University of Singapore, Singapore, 117542.*

⁴*Institute of High Performance Computing, 138632, Singapore*

(Dated: May 29, 2019)

Machine learning (ML) architectures such as convolutional neural networks (CNNs) have garnered considerable recent attention in the study of quantum many-body systems. However, advanced ML approaches such as gated recurrent neural networks (RNNs) have seldom been applied to such contexts. Here we demonstrate that a special class of RNNs known as long short-term memory (LSTM) networks is capable of learning and accurately predicting the time evolution of one-dimensional (1D) Ising model with simultaneous transverse and parallel magnetic fields, as quantitatively corroborated by relative entropy measurements and magnetization between the predicted and exact state distributions. In this unsupervised learning task, the many-body state evolution was predicted in an autoregressive way from an initial state, without any guidance or knowledge of any Hamiltonian. Our work paves the way for future applications of advanced ML methods in quantum many-body dynamics without relying on the explicit form of the Hamiltonian.

Introduction – Machine learning (ML) approaches, particularly neural networks (NNs), have achieved great success in solving real-world industrial and social problems [1], such as image recognition[2], high level image synthesis and style transfer[3], human-like raw speech generator[4], producing original melodious MIDI notes[5, 6], neural machine translation [7]. Inspired by its widespread applicability, ML was soon adopted by condensed matter physicists in the modeling of quantum many-body behavior and phase transition discovery [8–18]. Compared to so many advances in computer vision[19], speech processing[20], and natural language processing [21], it is natural to ask if recent progress in these more sophisticated ML architectures can benefit or even revolutionize the modeling of quantum systems. For instance, can quantum many-body dynamics be “learned” through unsupervised learning without knowing the explicit form of the Hamiltonian?

Thus, the main objective of this work is to demonstrate the novel application of Long Short-Term Memory (LSTM) neural networks in the unsupervised learning and prediction of the evolution of a many-body wavefunction, an otherwise computationally intensive task that has not been solved by generative models. Focusing on static problems, it is proven that deep NNs like restricted Boltzmann Machine (RBM) can represent most physical states[22], and a recent work based on very deep and large CNNs shows the ability to circumvent the need for Markov Chain sampling on two-dimensional interacting spin model of larger systems[23]. Lately, physical properties of spin Hamiltonians are reproduced by deep Boltzmann Machine (DBM), as an alternative to the standard path integral[24]. Our approach fundamentally contrasts

with conventional approaches in computing many-body dynamics: instead of evolving the wavefunction explicitly with the Hamiltonian, which becomes prohibitively slow as the number of spins increases, we directly predict the dynamical wavefunction from the initial state by propagating it with a LSTM network. Containing input, forget and output gates with fully-connected layers, LSTM networks are naturally suited for unsupervised learning of sequences [25], although they have never been harnessed for exact quantum state evolution, in our scenario, a 1D Ising model with both parallel and transverse magnetic field.

As a first demonstration, we specialize to the many-body dynamics of a one-dimensional (1D) Ising chain with transverse and parallel magnetic fields. Comparison with exact conventionally computed results with up to six spins reveal high predictive accuracy, as quantified by the relative entropy as well as magnetization. Indeed, our LSTM-propagated wavefunction showed a strong grasp of the periodicity in the time evolution, despite being unaware of the Hamiltonian that sets the energy (inverse periodicity) scale. We hope that such encouraging results from our pioneering unsupervised sequence learning approach to quantum many-body dynamics will also inspire other applications of state-of-art ML methods i.e. attention based model transformer[26] and explore more efficient data encoding methods to build a shared model suited for quantum systems with different spin variables. *Dynamics on a 1D Ising chain* – We consider a 1D Ising spin chain with local transverse (g) and parallel (h) magnetic fields, described by the Hamiltonian

$$H = - \sum_i \sigma_i^z \otimes \sigma_{i+1}^z - h \sum_i \sigma_i^z - g \sum_i \sigma_i^x. \quad (1)$$

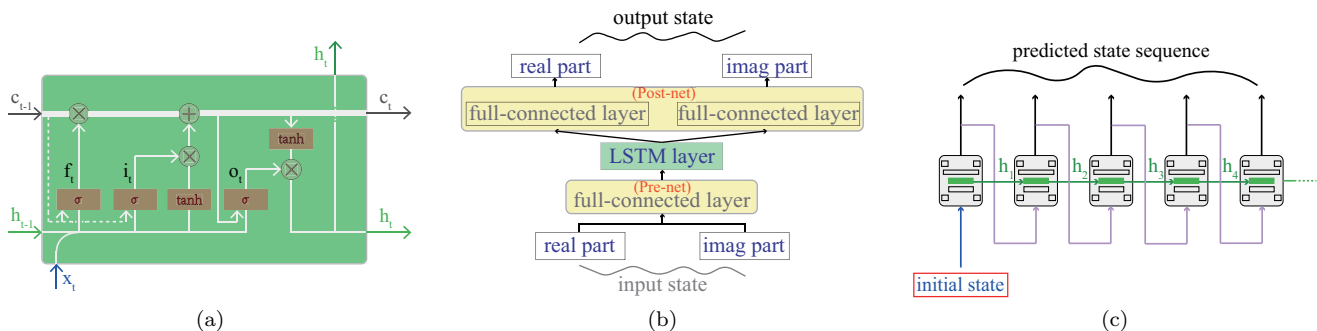


FIG. 1: (a) Details of a vanilla LSTM cell with input gate i_t , forget gate f_t , output gate o_t , memory cell (shown as white bold line) and peephole connections (shown as white dotted lines) from the previous memory cell c_{t-1} to both the forget gate f_t and input gate i_t . The forget gate decides what to forget from the previous memory cell c_{t-1} , the input gate decides what to read from the input and what to write into current memory cell c_t , and the output gate decides what to read from current memory cell c_t and what to output as h_t . The activation functions σ and \tanh are given by expressions $\sigma(x) = \frac{e^x}{e^x + 1}$ and $\tanh(x) = 2 \cdot \sigma(2x) - 1$. (b) Proposed architecture in our paper, which we take as a block composed of a Pre-net layer, a LSTM layer and a Post-net layer at each timestep. Pre-net and Post-net layers are both feed-forward layers. (c) Autoregressive procedure of generating new quantum states. Given an initial state at the beginning, each time-evolved quantum state is predicted from our proposed block by LSTM’s hidden information (shown as green arrows) and previous predicted state.

When the magnetic field is parallel ($g = 0$) or transverse ($h = 0$), the Hamiltonian is exactly solvable. However, when $g \neq 0$ and $h \neq 0$, the dynamics of N spins must be numerically computed in the 2^N -dimensional many-body Hilbert space spanned by direct product states Ψ of single-spin wavefunctions ψ_i :

$$\Psi = \prod_i^N \otimes \psi_i = \prod_i^N \otimes \begin{pmatrix} \phi_i^\uparrow \\ \phi_i^\downarrow \end{pmatrix}, \quad \dim \Psi = 2^N. \quad (2)$$

Wave function dynamics can be exactly computed through unitary time evolution of the Hamiltonian

$$|\Psi(t)\rangle = \exp\left(-i\frac{H}{\hbar}t\right)|\Psi(0)\rangle = V \exp\left(-i\frac{E}{\hbar}t\right)V^{-1}|\Psi(0)\rangle, \quad (3)$$

where $E = V^{-1}HV$ is the diagonal eigenenergy matrix.

The 2^N -dimensional N -body wave function $|\Psi(t)\rangle$ quickly becomes expensive to compute as N increases. We propose a ML approach with Pre-net, LSTM network, and Post-net, which instead attempts to predict its time evolution based on prior knowledge of the time evolution behavior of known training states. This training (learning) only has to be performed once for the relatively inexpensive prediction of any number of initial states. Importantly, the training and prediction process captures solely the intrinsic evolution patterns of the wavefunctions, and does not involve any explicit knowledge about the Hamiltonian. From the ML perspective, this dynamical state evolution problem can be regarded as a straightforward sequence generation problem [27].

The LSTM approach – We next outline the broad principles behind our LSTM approach of predicting quantum

state evolution, with details in [28]. LSTM can avoid the gradient diminishing problem [29] of RNN with its long-range dependencies in time due to its accessible, writable and erasable memory cells. These cells function as substantial aggregations of different states, which we use to encode the coherent evolution of quantum states. Here we choose the vanilla LSTM neural network with peephole connections (Fig.1a) which incorporates changes from Gers *et al.* [30] and Gers and Schmidhuber [31] into the original LSTM [32] and uses full gradient training, according to its better performance[33].

Our procedure occurs in two main stages: the training stage and the inference stage. In the training stage, we first “train” or optimize the weight parameters of our LSTM based network by feeding it with a large number of training sequences, which are the time-evolved wavefunction data of 10^5 randomly chosen initial 5 and 6-spin states sampled over 500 timesteps, obtained via conventional exact diagonalization (ED). The LSTM based network, including Pre-net and Post-net, is fully optimized by minimizing the mean squared error between the ED-evolved and LSTM-evolved states at all times.

Following the training stage is the inference stage, when the LSTM network is ready for predicting the evolution of arbitrarily given initial states. As sketched in Fig. 1c, the initial many-body state $|\Psi(t=0)\rangle$ enters the leftmost block at $t=0$, and its output is propagated as input state to the next block with hidden layers h_t . The output of each block denotes a new quantum state at a certain timestep. The combination of memory cell c_t and hidden output h_t serve to implement effective long-term and short-term “memory” behaviors respectively.

As illustrated in Fig. 1a and further elaborated in [28], relatively long-term information kept in memory cell c_t is modified by its previous value c_{t-1} , new input x_t interacted with input gate and forget gate at that timestep, as well as “hidden” information h_{t-1} from the previous LSTM cell. Besides c_t , each LSTM cell also outputs relatively short-term information h_t that will survive directly to both the Post-net and the next LSTM cell. Based on the already optimized LSTM based network, the predicted quantum state as a function of time would be generated from the Post-net of each block as shown in Fig. 1c.

Comparison between exact and LSTM based evolutions – We report very encouraging agreements between wavefunctions evolved by $e^{-iHt/\hbar}$ as computed by ED, and wavefunction evolutions as predicted by our LSTM based network. As for the Ising model, we set the local transverse magnetic field g to be -1.05 , parallel magnetic field g to be 0.5 and Δt , the time interval to be 0.002 , and keep this setting constant for all computation. We find that the maximum energy eigenvalue is about $0.1 \gg 0.002$, proving that the time interval we choose is small enough. The number of spins studied (5 and 6) decides the cost of exactly computing the 10^5 different time evolutions over 1 second (500 timesteps) prior to training the network, since the time complexity of ED method is $\mathcal{O}(2^n)$.

As a concrete demonstration, we visually illustrate the comparison for the evolution of a 5-spin and a 6-spin state in Fig. 2. These states are evolved from arbitrarily chosen typical initial states, as detailed in [28]. We compare the time evolutions of illustrative $|00101\rangle$ and $|000101\rangle$ components. Saliiently, the evolution predicted by the LSTM based model accurately reproduces that from exact computations at the beginning 200 timesteps. To confirm that this agreement is not just due to a fortuitous choice of component, we look at the evolution across all components of the same states in Fig. 3. We also show the error in Fig. 4 calculated along each state by

$$\text{Error} = 1 - \frac{|\langle \psi_{\text{ED}} | \psi_{\text{LSTM}} \rangle|}{\sqrt{\langle \psi_{\text{ED}} | \psi_{\text{ED}} \rangle \langle \psi_{\text{LSTM}} | \psi_{\text{LSTM}} \rangle}}. \quad (4)$$

As shown in Fig. 4a, We use gray dashed lines to mark the error rate every 100 timesteps. In general, the ED and LSTM-evolved states still agree well. In the five-spin system (red curve), the error rate is around 1% within the beginning 100 timesteps and around 3% within the total 500 timesteps; while in the six-spin system (green curve), the error rate is also around 1% within the beginning 100 timesteps and less than 4% within the total 500 timesteps. We can see that the errors are negligible after a considerable amount of time from the beginning.

To further quantify the agreement of LSTM and ED wavefunction evolutions, we compute the relative entropy (Kullback-Leibler divergence)[34] of their distributions over 1000 test wavefunctions sequences. For discrete probability distributions P and Q , the relative en-

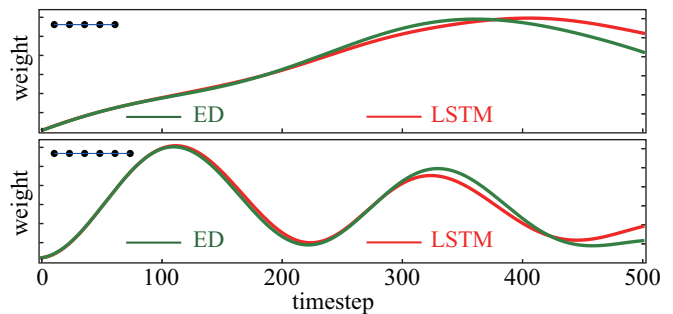


FIG. 2: Output (LSTM) and target (ED) wave function magnitude of $|00101\rangle$ and $|000101\rangle$ for both five and six-spin systems.

tropy is defined as

$$D_{KL}(P||Q) = \sum_x P(x) \log \left(\frac{P(x)}{Q(x)} \right). \quad (5)$$

Given ED-computed wavefunction coefficient vectors M^{ED} and LSTM-predicted coefficient vectors M^{LSTM} , the P and Q variables take values

$$P_{n,t,x} = \frac{|M_{n,t,x}^{\text{ED}}|}{\sum_{x=1}^{2^N} |M_{n,t,x}^{\text{ED}}|} \quad (6)$$

$$Q_{n,t,x} = \frac{|M_{n,t,x}^{\text{LSTM}}|}{\sum_{x=1}^{2^N} |M_{n,t,x}^{\text{LSTM}}|} \quad (7)$$

at time t and basis vector x , where n labels the test sequence. Hence the mean relative entropy at each timestep t is

$$D_{KL}(P||Q)(t) = \frac{1}{1000} \sum_{n=1}^{1000} \sum_{x=1}^{2^N} P_{n,t,x} \log \frac{P_{n,t,x}}{Q_{n,t,x}}, \quad (8)$$

and measures the amount of information lost when the distribution Q from LSTM predictions is used to represent the distribution P from ED results. The smaller the value of $D_{KL}(P||Q)(t)$, the more accurate is their agreement.

In Fig. 4b, we show how the mean relative entropy varies with time during the generation of test sequences. We find that in both systems, the order of relative-entropy is always within 0.04. Evidently, with the increase of timesteps, the relative entropy generally shows an upward trend, which is caused by the accumulation of errors in the process of conditional generation without any external guidance. To quantify our model’s performance by a physical variable, we draw the magnetization intensity calculated from both predicted (LSTM) and simulated (ED) wavefunctions in Fig. 5, which have a nice agreement.

Conclusion – In this work, we have successfully applied the unsupervised learning approach based on LSTM

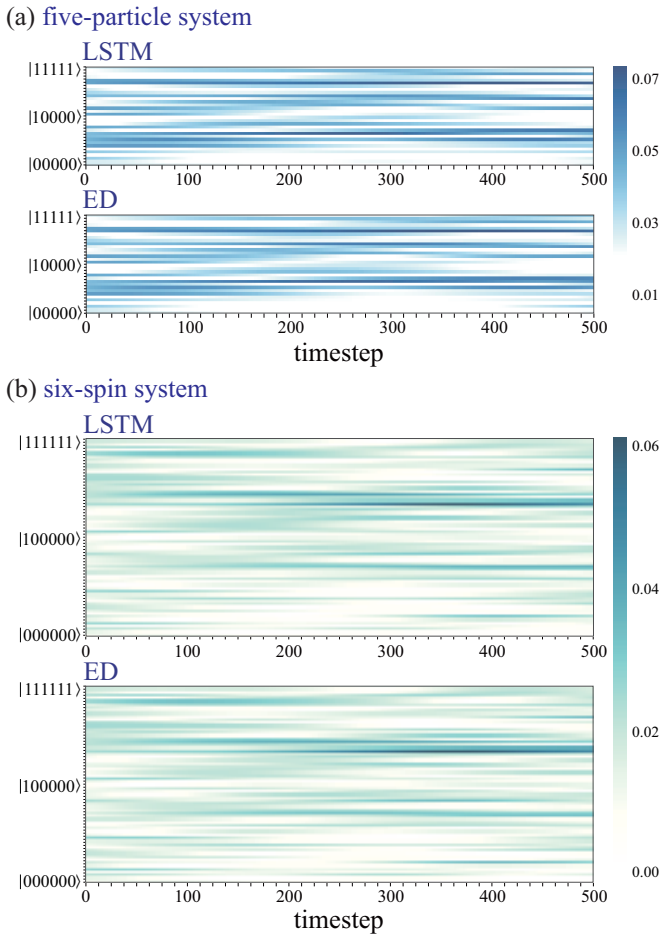


FIG. 3: Comparisons of all components of coefficients for LSTM based prediction and ED based simulation in each transverse lattice with different colors for both five-spin and six-spin systems.

networks to approximate the state evolution of dynamic quantum many-body systems with high accuracy. Our work encourages future applications of advanced ML methods in quantum many-body dynamics in a Hamiltonian-agnostic manner. Applications of these advancements in ML to quantum many-body problems are left to future work.

ACKNOWLEDGEMENTS

Xiao Zhang thanks Yingfei Gu, Meng Cheng, Yi Zhang for discussions. Xiao Zhang is supported by the National Natural Science Foundation of China (Grant No. 11874431), the National Key R & D Program of China (Grant No. 2018YFA0306800) and the Guangdong Science and Technology Innovation Youth Talent Program (Grant No. 2016TQ03X688). Shuo Yang is supported by NSFC (Grant No. 11804181), the National Key R & D Program of China (Grant No. 2018YFA0306504) and

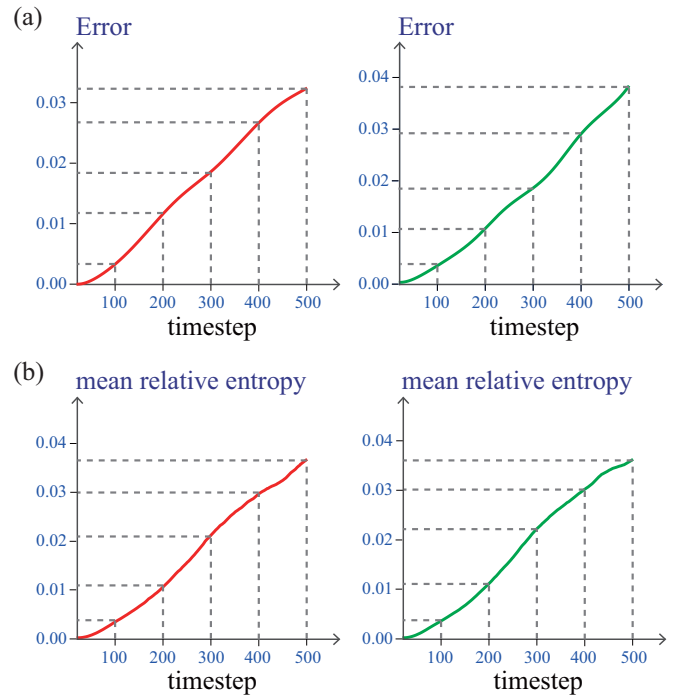


FIG. 4: (a) Error and (b) mean relative entropy of generating long sequences in both five (red curve) and six-spin system (green curve). The error and mean relative entropy increase linearly with timesteps in both systems.

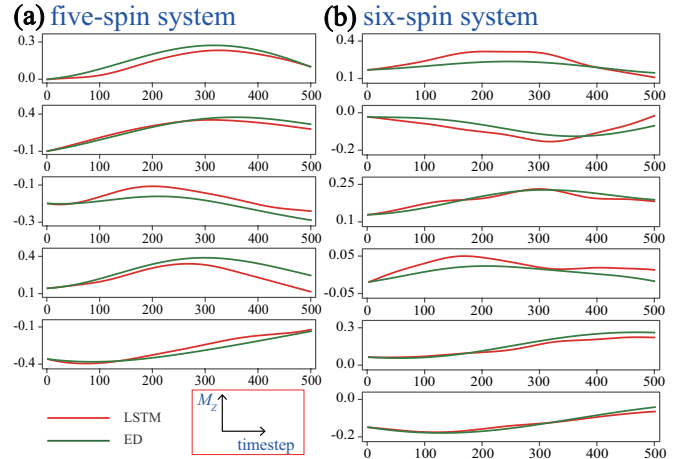


FIG. 5: Magnetization calculated by both LSTM (red curve) and ED (green curve) based wavefunctions for five and six-spin system.

the Research Fund Program of the State Key Laboratory of Low-Dimensional Quantum Physics (Grant No. ZZ201803).

* zhangxiao@mail.sysu.edu.cn

- [1] Y. Bengio, A. Courville, and P. Vincent, *IEEE transactions on pattern analysis and machine intelligence* **35**, 1798 (2013).
- [2] A. Krizhevsky, I. Sutskever, and G. E. Hinton, in *Advances in neural information processing systems* (2012) pp. 1097–1105.
- [3] L. A. Gatys, A. S. Ecker, and M. Bethge, in *Proceedings of the IEEE conference on computer vision and pattern recognition* (2016) pp. 2414–2423.
- [4] A. Van Den Oord, S. Dieleman, H. Zen, K. Simonyan, O. Vinyals, A. Graves, N. Kalchbrenner, A. Senior, and K. Kavukcuoglu, *CoRR* abs/1609.03499 (2016).
- [5] Z. Sun, J. Liu, Z. Zhang, J. Chen, Z. Huo, C. H. Lee, and X. Zhang, *arXiv preprint arXiv:1611.05416* (2016).
- [6] Z. Sun, J. Liu, Z. Zhang, J. Chen, Z. Huo, C. H. Lee, and X. Zhang, in *2018 Asia-Pacific Signal and Information Processing Association Annual Summit and Conference (APSIPA ASC)* (IEEE, 2018) pp. 1864–1867.
- [7] Y. Wu, M. Schuster, Z. Chen, Q. V. Le, M. Norouzi, W. Macherey, M. Krikun, Y. Cao, Q. Gao, K. Macherey, *et al.*, *arXiv preprint arXiv:1609.08144* (2016).
- [8] E. P. Van Nieuwenburg, Y.-H. Liu, and S. D. Huber, *Nature Physics* **13**, 435 (2017).
- [9] Z. Cai and J. Liu, *Physical Review B* **97**, 035116 (2018).
- [10] G. Torlai and R. G. Melko, *Physical Review B* **94**, 165134 (2016).
- [11] G. Torlai and R. G. Melko, *Physical review letters* **119**, 030501 (2017).
- [12] D.-L. Deng, X. Li, and S. Das Sarma, *Phys. Rev. X* **7**, 021021 (2017).
- [13] J. Gray, L. Banchi, A. Bayat, and S. Bose, *Physical review letters* **121**, 150503 (2018).
- [14] K. Chng, J. Carrasquilla, R. G. Melko, and E. Khatami, *Physical Review X* **7**, 031038 (2017).
- [15] P. Broecker, J. Carrasquilla, R. G. Melko, and S. Trebst, *Scientific reports* **7**, 8823 (2017).
- [16] M. H. Amin, E. Andriyash, J. Rolfe, B. Kulchytskyy, and R. Melko, *Physical Review X* **8**, 021050 (2018).
- [17] Y. Zhang and E.-A. Kim, *Physical review letters* **118**, 216401 (2017).
- [18] G. Carleo and M. Troyer, *Science* **355**, 602 (2017).
- [19] A. Voulodimos, N. Doulamis, A. Doulamis, and E. Protopapadakis, *Computational intelligence and neuroscience* **2018** (2018).
- [20] L. Deng, G. Hinton, and B. Kingsbury, in *2013 IEEE International Conference on Acoustics, Speech and Signal Processing* (IEEE, 2013) pp. 8599–8603.
- [21] T. Young, D. Hazarika, S. Poria, and E. Cambria, *IEEE Computational Intelligence Magazine* **13**, 55 (2018).
- [22] X. Gao and L.-M. Duan, *Nature communications* **8**, 662 (2017).
- [23] O. Sharir, Y. Levine, N. Wies, G. Carleo, and A. Shashua, *arXiv preprint arXiv:1902.04057* (2019).
- [24] G. Carleo, Y. Nomura, and M. Imada, *Nature communications* **9**, 5322 (2018).
- [25] A. Graves, *arXiv preprint arXiv:1308.0850* (2013).
- [26] A. Vaswani, N. Shazeer, N. Parmar, J. Uszkoreit, L. Jones, A. N. Gomez, L. Kaiser, and I. Polosukhin, in *Advances in neural information processing systems* (2017) pp. 5998–6008.
- [27] I. Sutskever, O. Vinyals, and Q. V. Le, in *Advances in neural information processing systems* (2014) pp. 3104–3112.
- [28] Supplemental Online Material (2019).
- [29] R. Pascanu, T. Mikolov, and Y. Bengio, in *International Conference on Machine Learning* (2013) pp. 1310–1318.
- [30] F. A. Gers, J. Schmidhuber, and F. Cummins, (1999).
- [31] F. A. Gers and J. Schmidhuber, in *Proceedings of the IEEE-INNS-ENNS International Joint Conference on Neural Networks. IJCNN 2000. Neural Computing: New Challenges and Perspectives for the New Millennium*, Vol. 3 (IEEE, 2000) pp. 189–194.
- [32] S. Hochreiter and J. Schmidhuber, *Neural computation* **9**, 1735 (1997).
- [33] K. Greff, R. K. Srivastava, J. Koutník, B. R. Steunebrink, and J. Schmidhuber, *IEEE transactions on neural networks and learning systems* **28**, 2222 (2017).
- [34] V. Vedral, *Reviews of Modern Physics* **74**, 197 (2002).
- [35] R. Moessner, S. L. Sondhi, and P. Chandra, *Physical Review Letters* **84**, 4457 (2000).
- [36] D. P. Kingma and J. Ba, *arXiv preprint arXiv:1412.6980* (2014).
- [37] M. Abadi, P. Barham, J. Chen, Z. Chen, A. Davis, J. Dean, M. Devin, S. Ghemawat, G. Irving, M. Isard, *et al.*, in *12th {USENIX} Symposium on Operating Systems Design and Implementation ({OSDI} 16)* (2016) pp. 265–283.

Supplemental Online Material for “Predicting quantum many-body dynamics with Long Short-Term Memory based neural networks”

In this supplementary material, we detail: 1) the key equations of adopted LSTM cell 2) the algorithm of training our proposed LSTM based quantum many-body network, 3) the training procedure of our LSTM based quantum many-body network, 4) the initial quantum states used for prediction.

Appendix A: Details of LSTM based NN

The LSTM cell we adopted is shown in Fig.1(a), below we list the key equations of our LSTM:

$$\begin{aligned}
 i_t &= \sigma(W_{xi}x_t + W_{hi}h_{t-1} + W_{ci}c_{t-1} + b_i) \\
 f_t &= \sigma(W_{xf}x_t + W_{hf}h_{t-1} + W_{cf}c_{t-1} + b_f) \\
 c_t &= f_t c_{t-1} + i_t \tanh(W_{xc}x_t + W_{hc}h_{t-1} + b_c) \quad (\text{A1}) \\
 o_t &= \sigma(W_{xo}x_t + W_{ho}h_{t-1} + W_{co}c_t + b_o) \\
 h_t &= o_t \tanh(c_t)
 \end{aligned}$$

Once a new input comes, the input gate i_t decides whether to accumulate its information to the memory cell c_{t-1} ; also, if the forget gate f_t is activated, the previous cell status c_{t-1} may be partially forgotten; to this end, the output gate o_t decides how to transmit the latest cell c_t to the hidden state h_t . In this way, LSTM with information flow renders the sequence generation problem to be more reasonably tackled.

To predict our model dynamic process for the quantum many-body Ising type 1-D system, we propose a new layered hierarchical model composed of Pre-net, one LSTM layer and Post-net (see Fig.1(b)). LSTM with peephole connections, the memory cell decides what to store, and when to read, write and erase via several differential gates. Both Pre-net and Post-net are composed of full-connected layers, with full working scheme are as follows. First we adroitly stack up the real and imaginary part of each complex coefficient as input. To extract more abundant latent information, we feed the input into Pre-net composed of a 512-unit full-connected layer with \tanh activation function. Then, the high dimensional feature is passed through the LSTM layer with 512 hidden neurons to make full use of long-context information. Finally, the output of LSTM layer is converted to the real and imaginary part of state coefficients by Post-net, each by a 512-unit full-connected layer with linear activation function.

At the stage of training (Fig. A1), given a state sequence of n timesteps $\{\Psi_1, \dots, \Psi_n\}$, we can split it into two subsequences: $seq_i = \{\Psi_1, \Psi_2, \dots, \Psi_{n-2}, \Psi_{n-1}\}$ and $seq_o = \{\Psi_2, \Psi_3, \dots, \Psi_{n-1}, \Psi_n\}$. Then we adopt an unsupervised learning method which passes the input seq_i into the network at each timestep, and computes output seq_o of the final layer based on a linear activation function. In contrast, at the stage of inference (Fig.1(c)), we only pass the initial wave function into the network as input, and auto-regressively generates the following states at future timesteps, by consuming the previously generated states

as additional input. The full procedure of training and inference is detailed in Algorithm 1.

Algorithm 1 Learning quantum many-body dynamics by long short-term memory network

Require: θ : the parameters of whole network composed of Pre-net, LSTM and Post-net.

Input: B_S coefficient sequences in a batch with T_L timesteps each.

Output: same as input but with one timestep offset.

Preparation: concatenate the real part x_r and imaginary part x_i of each complex coefficient into x .

Training Stage:

```

1: Initialize  $\theta$ 
2: for each training epoch do
3:   for  $k$  steps do
4:     obtain the output of Pre-net:
5:      $output_r = \tanh(W_r x + b_r)$ 
6:     pass through LSTM cell:
7:      $output_l = \text{LSTM}(output_r)$ 
8:     obtain the real part of output coefficient from Post-net:
9:      $c_r = \text{linear}(W_{o1} output_l + b_{o1})$ 
10:    obtain the imaginary part of output coefficient from Post-net:
11:     $c_i = \text{linear}(W_{o2} output_l + b_{o2})$ 
12:    Update  $\theta$  by ascending the stochastic gradient descent:
13:     $\nabla(\theta) \left\{ \frac{1}{T_L} \sum_{T_L} \frac{1}{B_S} \sum_{B_S} [(x_r - c_r)^2 + (x_i - c_i)^2] \right\}$ 
14:  end for
15: end for

```

Inference Stage:

```

16: for  $g$  steps do
17:   if  $g == 1$  then
18:     compute the first predicted coefficient vector  $c_1$  by feeding with initial coefficient sequence as input:
19:      $c_1 = \text{network}(input; \theta)$ 
20:   else
21:     compute new coefficients  $c_g$  by feeding with previous output  $c_{g-1}$ :
22:      $c_g = \text{network}(c_{g-1}; \theta)$ 
23:   end if
24: end for

```

To be more explicit, our dataset is gathered by computing the time evolution of wave functions from the five and six-spin systems every 0.002 second, using exact diagonalization (ED) method[35]. Treated as a standard ML process, we divide the whole dataset into three parts: a training set with 100,000 sequences, a valida-

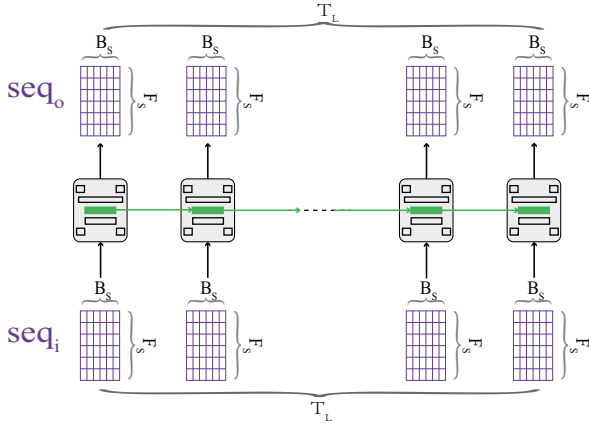


FIG. A1: During the training stage, we takes the current wave functions as input and next state as the ground label. Notably, the ground label sequence is one timestep off the input sequence.

System	five-spin	six-spin
input dimension	[100, 500, 64]	[100, 500, 128]
hidden neurons of Pre-net	64	128
hidden neurons of LSTM	512	512
hidden neurons of Post-net	64	128
output dimension	[100, 500, 64]	[100, 500, 128]

TABLE A1: Different neurons used for training the five and six-spin system.

tion set with 1000 sequences and a test set with 1000 sequences. During training, we use the mini-batch gradient descent framework to optimize our network and $m = 100$ is the batch size (B_S) we use, considering both NN's convergence speed and GPU memory. As shown in Fig A1, our network receives an input sequence $[B_S, T_L, F_S]$ during training. T_L is the length of different timesteps and each sequence contains 501 complex-valued quantum states over a continuous period of one second. F_S is twice the dimension of wave function basis, by separating real and imaginary parts. For five and six-spin systems, $[T_L, F_S]$ are $[501, 2^5 \times 2]$ and $[501, 2^6 \times 2]$, respectively. By splitting the 501 timesteps into two subsequences: $seq_i = \{\Psi_1, \Psi_2, \dots, \Psi_{n-2}, \Psi_{n-1}\}$ and $seq_o = \{\Psi_2, \Psi_3, \dots, \Psi_{n-1}, \Psi_n\}$ with one timestep offset, the input and output data format for training are $[100, 500, 64]$ and $[100, 500, 128]$ for five and six-spin systems, respectively. As a last reminder, systems with different number of spins have different Pre-net and Post-net dimensions. The aforementioned data formats are summarized in Table A1.

Appendix B: Training procedure

The target of training is to minimize the mean squared error (MSE) at all timesteps between output and target states. Before training, we initialize all weight variables based on normal distribution and set all bias variables to be zero vectors. We use the adaptive moment estimation (Adam) optimizer [36] to update the parameters for that it's very suitable for tasks with datasets of large dimension and needs less memory space, with an initial learning rate of 0.001 decayed by a factor of 0.99 every epoch until the learning rate falls below $5.0e-5$. We train our model for 300 epoches and keep the best model with a lowest validation loss. Our model is implemented in TensorFlow framework [37] and all simulations are run on single NVIDIA QUODRA K5200 GPU. For the five and six-spin systems, the training costs 24 and 48 hours, respectively.

Appendix C: Initial states used for prediction

1. The initial state of five-spin system for sequence generation

$$\begin{aligned}
& (0.075+0.102i)|00000\rangle + (0.072+0.056i)|00001\rangle \\
& + (-0.053+0.085i)|00010\rangle + (-0.103+0.050i)|00011\rangle \\
& + (0.081+0.258i)|00100\rangle + (0.103+0.250i)|00101\rangle \\
& + (0.020+0.052i)|00110\rangle + (-0.131+0.067i)|00111\rangle \\
& + (-0.101+0.153i)|01000\rangle + (-0.060+0.214i)|01001\rangle \\
& + (-0.123+0.028i)|01010\rangle + (0.012+0.096i)|01011\rangle \\
& + (-0.022+0.111i)|01100\rangle + (-0.100+0.259i)|01101\rangle \\
& + (0.048+0.087i)|01110\rangle + (-0.020+0.264i)|01111\rangle \\
& + (-0.064+0.019i)|10000\rangle + (-0.019+0.040i)|10001\rangle \\
& + (0.048+0.000i)|10010\rangle + (-0.101+0.238i)|10011\rangle \\
& + (-0.108+0.081i)|10100\rangle + (0.073+0.212i)|10101\rangle \\
& + (-0.112+0.197i)|10110\rangle + (0.088+0.222i)|10111\rangle \\
& + (-0.048+0.213i)|11000\rangle + (-0.093+0.261i)|11001\rangle \\
& + (-0.050+0.042i)|11010\rangle + (-0.115+0.172i)|11011\rangle \\
& + (-0.048+0.008i)|11100\rangle + (-0.112+0.165i)|11101\rangle \\
& + (-0.073+0.115i)|11110\rangle + (-0.039+0.132i)|11111\rangle
\end{aligned}$$

2. The initial state of six-spin system for sequence generation

$$\begin{aligned}
& (0.001+0.154i)|000000\rangle + (-0.011+0.146i)|000001\rangle \\
& + (-0.095+0.073i)|000010\rangle + (0.057+0.169i)|000011\rangle \\
& + (-0.056+0.063i)|000100\rangle + (0.057+0.186i)|000101\rangle \\
& + (0.089+0.046i)|000110\rangle + (-0.021+0.141i)|000111\rangle \\
& + (-0.054+0.088i)|001000\rangle + (-0.048+0.151i)|001001\rangle \\
& + (-0.097+0.057i)|001010\rangle + (-0.043+0.038i)|001011\rangle \\
& + (-0.048+0.175i)|001100\rangle + (0.023+0.190i)|001101\rangle \\
& + (-0.063+0.147i)|001110\rangle + (0.084+0.108i)|001111\rangle \\
& + (-0.046+0.146i)|010000\rangle + (0.035+0.160i)|010001\rangle
\end{aligned}$$

$+(0.081+0.141i)|010010\rangle+(0.087+0.141i)|010011\rangle$
 $+(-0.052+0.134i)|010100\rangle+(0.012+0.187i)|010101\rangle$
 $+(-0.028+0.108i)|010110\rangle+(-0.069+0.051i)|010111\rangle$
 $+(0.032+0.023i)|011000\rangle+(0.013+0.098i)|011001\rangle$
 $+(0.034+0.099i)|011010\rangle+(0.032+0.023i)|011011\rangle$
 $+(0.073+0.007i)|011100\rangle+(0.007+0.026i)|011101\rangle$
 $+(0.018+0.194i)|011110\rangle+(-0.048+0.096i)|011111\rangle$
 $+(-0.054+0.023i)|100000\rangle+(0.060+0.046i)|100001\rangle$
 $+(-0.048+0.086i)|100010\rangle+(-0.086+0.048i)|100011\rangle$
 $+(0.008+0.101i)|100100\rangle+(-0.047+0.182i)|100101\rangle$
 $+(0.051+0.104i)|100110\rangle+(0.089+0.006i)|100111\rangle$
 $+(0.084+0.001i)|101000\rangle+(0.094+0.080i)|101001\rangle$

$+(0.049+0.068i)|101010\rangle+(0.026+0.137i)|101011\rangle$
 $+(0.004+0.031i)|101100\rangle+(0.025+0.036i)|101101\rangle$
 $+(-0.066+0.084i)|101110\rangle+(-0.044+0.005i)|101111\rangle$
 $+(-0.052+0.082i)|110000\rangle+(0.080+0.190i)|110001\rangle$
 $+(-0.001+0.110i)|110010\rangle+(0.063+0.056i)|110011\rangle$
 $+(0.002+0.041i)|110100\rangle+(-0.064+0.123i)|110101\rangle$
 $+(-0.050+0.148i)|110110\rangle+(0.093+0.047i)|110111\rangle$
 $+(0.038+0.009i)|111000\rangle+(-0.020+0.142i)|111001\rangle$
 $+(-0.082+0.068i)|111010\rangle+(0.083+0.184i)|111011\rangle$
 $+(-0.059+0.016i)|111100\rangle+(0.026+0.160i)|111101\rangle$
 $+(-0.084+0.069i)|111110\rangle+(0.051+0.047i)|111111\rangle$